Journal of Catalysis **206,** 339–348 (2002)
doi:10.1006/jcat.2001.3494, available online at http://www.idealibrary.com on IDEAL®

Effect of Sb/V Ratio and of Sb + V Coverage on the Molecular Structure and Activity of Alumina-Supported Sb–V–O Catalysts for the Ammoxidation of Propane to Acrylonitrile

M. O. Guerrero-Pérez,* J. L. G. Fierro,* M. A. Vicente,† and M. A. Bañares*,[1]

*Instituto de Catálisis y Petroleoquímica, CSIC, Campus UAM-Cantoblanco, E-28049-Madrid, Spain; and †Departamento de Química Inorgánica, Universidad de Salamanca, Pza. Merced s/n, E-37008-Salamanca, Spain

Received September 14, 2001; revised December 14, 2001; accepted December 14, 2001

The effect of the total coverage of Sb + V oxides and the effect of the Sb/V atomic ratio on the ammoxidation of propane to acrylonitrile on alumina-supported V and Sb oxide catalysts is reported. The fresh and used catalysts are characterized by XRD and *in situ* Raman spectroscopy. Comparison with binary V–Al–O and Sb–Al–O catalysts shows that the presence of both Sb and V oxides strongly enhances the rate of propane ammoxidation to acrylonitrile on alumina-supported Sb–V oxide catalysts. The stability and structural changes during on-stream operation prior to reach steady-state operation originates from a close interaction between Sb and V oxides. The Sb–V interaction depends on total Sb + V coverage on alumina. Below the dispersion limit, $SbVO_4$ phases are not stable under reaction and break into the individual oxides. At Sb + V loading beyond dispersion limit, $SbVO_4$ phases are stable under reaction conditions while Sb and V oxides that did not combine during calcination of the precursor recombine into $SbVO_4$ phases. This solid-state reaction accounts for a higher propane conversion and selectivity to acrylonitrile. Comparison of the performance and molecular structures of fresh and used catalysts further suggests that Sb–V–O phases are necessary for this reaction. The specific formation of acrylonitrile per vanadium site reaches a maximum at an atomic Sb/V ratio of 2. It is likely that a moderate excess of antimony may be necessary for an efficient ammoxidation of propane to acrylonitrile.

Key Words: **V–Sb–Al-oxides; oxidation; ammoxidation; propane; acrylonitrile; structure–activity relationship; coverage; *in situ* Raman; XRD.**

INTRODUCTION

The direct conversion of propane into acrylonitrile by reaction with oxygen and ammonia is an alternative route to the conventional propylene ammoxidation since propylene is several times more expensive than propane. The economic implications of this new route are very important. Thus, in 1997 British Petroleum started a demonstration plant to make acrylonitrile, using propane, and estimated to decrease production costs ca. 20% compared with conventional propylene-based technology (1). In this reaction, the activation of propane is the limiting step. Since the adsorption rate of propane is near ten times smaller than that of propylene (2), the conversion of propane is at least ten times smaller than that of propylene (3). The reaction conditions to activate the C–H bond in propane are more energy demanding, which has a negative effect on selectivity. The use of homogeneous–heterogeneous processes to promote propane to propylene conversion upstream the catalyst bed is an option (4). However, other side products may be generated in the gas phase, like ammonia oxidation to nitrogen in the presence of molecular oxygen (5). The low activity of propane has also led to the use of gas phase additives (e.g., H_2S or CH_3Br) as radical generators. However, environmental concerns do not make this option attractive. Therefore, the efforts focus on a catalyst for the direct ammoxidation of propane into acrylonitrile with no additives in the gas phase.

Efficient catalysts for propane ammoxidation are based on antimony or molybdenum (6). Most of the reported work is concentrated on antimony-based catalysts, like vanadium antimonates with rutile structure (7–10) or on molybdenum (11–15). The molybdates can be promoted with Bi (11). Some molybdates may possess scheelite structure (12–14). Mo–V catalysts modified with Nb and Te may afford near 50% yield to acrylonitrile (15). On Sb–V–O based catalysts, the presence of alumina endows the system with better performance (14, 16). Despite the large relevance of these catalysts, the nature of the active site is still not fully understood. Sb–V–O catalysts with an excess of V are highly active and selective for propane oxidative dehydrogenation (ODH) while an excess of Sb affords Sb–V–O catalysts more efficient for propane ammoxidation (16).

The catalysts show adsorption of both ammonia and propane (3, 17–19). However, different catalyst formulations may lead to different limiting steps in the reaction route. Molybdate catalysts appear to be limited by propane

[1] To whom correspondence should be addressed. E-mail: mbanares@icp.csic.es.

0021-9517/02 $35.00

activation while antimonate catalysts appear to be limited by ammonia activation (20). Propane is likely to react via a hydrogen abstraction from a single methylene group followed by removal of a hydrogen from a primary carbon in a subsequent step (21). The presence of ammonia makes the reaction more selective since intermediate propylene is proposed to further react with ammonia to form acrylonitrile, which is more stable and undergoes minor degree of oxidative degradation (22). Transient experiments show that short-lived NHx fragments are active species in the formation of acrylonitrile from propane (19). IR studies suggest a competitive adsorption of ammonia during ammoxidation reaction (8). Oxygen is provided through the lattice of the oxide and molecular oxygen regenerates the catalyst (3). Recent transient studies confirm this trend for Sb–V–O catalysts (23).

The details on the structure and nature of surface species on Sb–V–Al mixed metal oxide catalysts is not fully understood due to the lack of stoichiometry of the $SbVO_4$ phases and the role of surface enrichment with Sb or V species. This work presents a study of model alumina-supported Sb–V–O catalysts. The effect of total Sb + V coverage on alumina and the effect of atomic Sb/V ratio are evaluated on the activity/selectivity for propane ammoxidation to acrylonitrile. The structure is characterized by XRD and *in situ* dispersive Raman spectroscopy. The combination of model catalysts, characterization, and activity is used to provide information about the structure-activity/selectivity relationship in vanadium antimonate catalysts for propane ammoxidation.

EXPERIMENTAL AND METHODS

Preparation of Samples

The Al–Sb–V–oxide catalysts were prepared by the following slurry method. Sb_2O_3 (Aldrich) was added to an aqueous solution of NH_4VO_3 (Sigma). This solution was kept under stirring at 80°C for 50 min and then γ-Al_2O_3 powder was added. The resulting dissolution was dried in a rotatory evaporator at 80°C. The resulting solid was dried at 115°C for 24 h and then calcined at 400°C for 4 h. When only two of the elements Al and Sb or Al and V are included in the preparation, the same procedure was used with the necessary modifications. The catalysts were prepared so that a total coverage of V + Sb would correspond to 25, 50, 100% and twice their dispersion limit on alumina. The dispersion limit, understood as the maximum surface loading of VO_x units that remain dispersed, with no crystalline V_2O_5, was determined by Raman spectroscopy to be near 9 VOx units per nm^2 of alumina support, in accordance with previous reports on another alumina (24). The Sb/V atomic ratio changed in the 1–5 interval.

For the sake of simplicity, all the alumina-supported catalysts are labeled as "xV_ySb–Al" where x represents the fraction of dispersion limit ("monolayer" coverage) of V + Sb atoms on alumina and y represents the Sb/V ratio. Reference catalysts with no Sb or no V were also prepared (1Sb–Al and 1V–Al, respectively). For comparative purposes, reference α-Sb_2O_4 was obtained from Sb_2O_3 after calcining in air for 30 h at 800°C. It was characterized by Raman spectroscopy and XRD. Reference $SbVO_4$ was obtained by liofilization method of a NH_4VO_3 and Sb_2O_3 solution in acid medium. The precursor was calcined at 800°C.

Characterization

Nitrogen adsorption isotherms (−196°C) were recorded on an automatic Micromeritics ASAP-2000 apparatus. Prior to the adsorption experiments, samples were outgassed at 413 K for 2 h. BET areas were computed from the adsorption isotherms ($0.05 < P/Po < 0.27$), taking a value of 0.164 nm^2 for the cross-section of the adsorbed N_2 molecule at −196°C. X-ray diffraction patterns were recorded on a Siemens Krystalloflex D-500 diffractometer using Cu $K\alpha$ radiation ($\lambda = 0.15418$ nm) and a graphite monochromator. Working conditions were 40 kV, 30 mA, and scanning rate of 2°/min for Bragg's angles (2θ) from 5 to 70°. In some cases, the peaks of Al from the sample holder are present.

Raman spectra were run with a single monochromator Renishaw System 1000 equipped with a cooled CCD detector (−73°C) and holographic super-Notch filter. The holographic Notch filter removes the elastic scattering while the Raman signal remains very high. The samples were excited with the 514 nm Ar line; spectral resolution was ca. 3 cm^{-1} and spectrum acquisition consisted of 20 accumulations of 30 s. The spectra were obtained under dehydrated conditions (ca. 120°C) in a hot stage (Linkam TS-1500). Hydrated samples were obtained at room temperature after and under exposure to a stream of humid synthetic air.

Activity Measurements

Activity measurements were performed using a conventional microreactor with on-line gas chromatograph equipped with a flame ionization and thermal conductivity detectors. The correctness of the analytical determinations was checked for each test by verification that the carbon balance (based on the propane converted) was within the cumulative mean error of the determinations (±10%). To prevent participation of homogeneous reactivity (4) the reactor was designed to minimize gas-phase activation of propane. Tests were made using 0.2 g of sample with particle dimensions in the 0.25–0.125 mm range. The axial temperature profile was monitored by a thermocouple sliding inside a tube inserted into the catalytic bed. Tests were made using the following feedstock: 25% O_2, 9.8% propane, 8.6% ammonia in helium. These proportions were selected in order to obtain a O_2/He ratio similar to that of O_2/N_2 in the air. The total flow rate was 20 ml/min corresponding to a gas-space velocity (GHSV) of about 3000 h^{-1}. Yields and

TABLE 1

Composition and BET Area of Alumina-Supported Sb–V–O Catalysts

Sb + V "monolayer"	Sb/V atomic ratio	Catalyst	% Sb	% V	BET Area m^2/g
0.25	5	$0.25Sb_5V$–Al	5.06	0.42	147
0.50	5	$0.5Sb_5V$–Al	9.40	0.76	139
	1	$1Sb_1V$–Al	10.13	4.20	118
	2	$1Sb_2V$–Al	13.38	2.77	117
	3	$1Sb_3V$–Al	15.00	2.11	121
1					
	4	$1Sb_4V$–Al	15.98	1.68	118
	5	$1Sb_5V$–Al	17.60	1.45	128
	7	$1Sb_7V$–Al	16.90	1.04	119
	1	$2Sb_1V$–Al	16.70	6.97	91
	3	$2Sb_3V$–Al	24.67	3.41	106
2					
	5	$2Sb_5V$–Al	26.79	2.37	78
	7	$2Sb_7V$–Al	28.26	1.71	93

selectivities in products were determined on the basis of the moles of propane feed and products, considering the number of carbon atoms in each molecule.

RESULTS

BET Area

The BET surface areas of the catalyst are listed in the Table 1. The BET area values decrease with surface coverage of Sb + V on Al_2O_3 from ca. 150 to 100 m^2/g. The atomic Sb/V ratio does not appear to have a clear effect on BET area values.

XRD

Figure 1 shows the X-ray diffraction patterns of reference compounds $SbVO_4$ (JCPDS file 16-0600), V_2O_5 (JCPDS file 41-1426), Sb_2O_3 (JCPDS file 11-689), and α-Sb_2O_4 (JCPDS file 11-694), which correspond to those of JCPDS data bases.

Figure 2 shows the X-ray diffraction patterns of reference catalysts 1V–Al and 1Sb–Al and of catalysts $0.25Sb_5V$–Al and $0.50Sb_5V$–Al. 1V–Al shows two broad patterns near 45.8, 66.8, 31.2, 25.9, and 20.2°, characteristic of alumina support (JCPDS file 37-1462). Fresh 1V–Al shows a weak pattern of V_2O_5, which is absent in used 1V–Al. 1Sb–Al catalyst shows the alumina pattern along with sharper diffraction peaks at 25.8, 29.0, 30.4, 33.8, and 37.4°, characteristic of α-Sb_2O_4. No significant changes are evident to XRD on used 1Sb. On the other hand, $0.25Sb_5V$–Al and $0.50Sb_5V$–Al show the diffraction patterns of Sb_2O_3 and of α-Sb_2O_4, along with broad peaks of alumina support. After catalytic runs on $0.25Sb_5V$–Al and $0.50Sb_5V$–Al only α-Sb_2O_4 phase is evident to XRD.

Figure 3 shows the diffraction patterns of fresh and used alumina-supported Sb–V–O catalyst at its dispersion limit loading on alumina for variable Sb/V atomic ratios. The used catalysts show some changes. At Sb + V dispersion limit loading, Sb_2O_3 phase tends to disappear and, in most cases, the presence of α-Sb_2O_4 decreases. The interaction between Sb and V phase is evidenced for 2 Sb/V that forms $SbV_{1-x}O_{4-1.5x}$ phases after its operation in propane ammoxidation reaction. Below Sb + V dispersion limit loading, fresh catalysts show Sb_2O_3 phase, which is removed during on-stream operation.

Figure 4 shows the diffraction patterns of fresh and used alumina-supported Sb–V–O catalyst at twice the dispersion limit loading on alumina Sb/V atomic ratio. In no case, the catalysts show the diffraction pattern of crystalline V_2O_5, most likely due to the excess of Sb. At high Sb/V atomic ratio, only Sb_2O_3 and α-Sb_2O_4 are evident to XRD. $2Sb_7V$–Al exhibits an increase of α-Sb_2O_4 phase after its use in reaction. When Sb/V atomic ratio is 5 ($2Sb_5V$–Al), reaction leads to an amorphization of the system, according to XRD patterns. If the ratio is lower ($2Sb_3V$–Al), fresh catalyst show α-Sb_2O_4 that decreases after use in reaction and a new phase becomes evident. On $2Sb_1V$–Al, $SbVO_4$, and

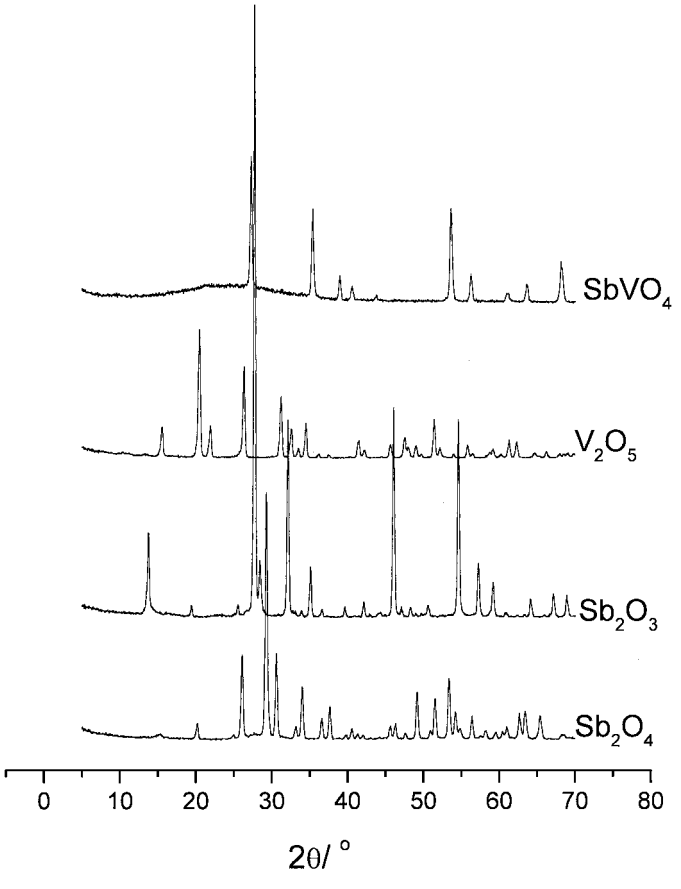

FIG. 1. XRD patterns of reference samples: α-Sb_2O_4, Sb_2O_3, V_2O_5, and $SbVO_4$,

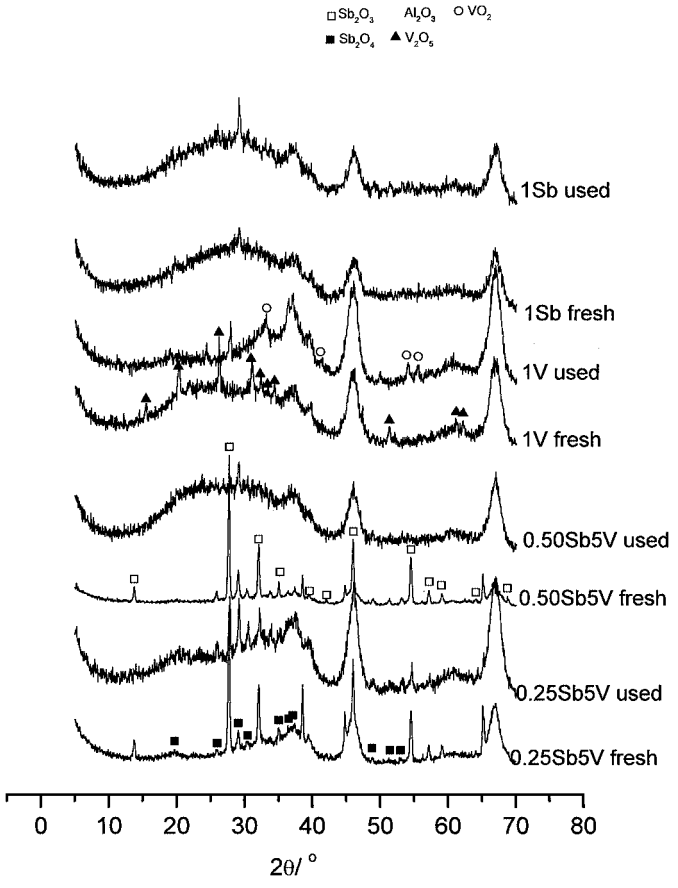

FIG. 2. XRD patterns of fresh and used 1V–Al, 1Sb–Al, $0.25Sb_5V$–Al, and $0.50Sb_5V$–Al catalysts.

α-Sb_2O_4 phases are present in the fresh catalyst. After its use in reaction, $SbVO_4$ phase increases at the expense of α-Sb_2O_4. In all systems, catalytic on-stream operation appears to oxidize Sb(III) to Sb(IV) in α-Sb_2O_4 or Sb(V) in $SbVO_4$ phases. While the oxidation state of vanadium appears to decrease to V(IV), as $SbVO_4$ phases. The oxidation states in $SbVO_4$ phases appear to be Sb(V) and V(III) (25).

Raman Spectroscopy

Figure 5 displays the Raman spectra of reference compounds Sb_2O_3, α-Sb_2O_4, $SbVO_4$, and V_2O_5. Sb_2O_3 shows Raman bands at 190, 255, 372, 451, and 716 cm^{-1} while for α-Sb_2O_4 Raman bands appear at 190, 261, 399, and 459 cm^{-1}. Pure V_2O_5 exhibits Raman bands at 143, 283, 302, 405, 480, 526, 698, and 994 cm^{-1}. $SbVO_4$ shows a broad band between 700 and 900 cm^{-1}, it also presented bands that correspond to Sb_2O_4, as in agreement with its XRD pattern that presented diffraction patterns for $SbVO_4$ and Sb_2O_4 phases.

Figure 6 shows the Raman spectra of dehydrated catalysts 1V–Al and 1Sb–Al along with those of catalysts $0.25Sb_5V$–Al and $0.50Sb_5V$–Al. Fresh dehydrated 1V–Al shows Raman bands at 1024 and 887 cm^{-1}, characteristic of the V=O and V–O–V modes of surface VOx species, respectively. No Raman bands of V_2O_5 phase are recorded. Dehydrated 1Sb–Al has very weak Raman bands that correspond to α-Sb_2O_4. Fresh $0.25Sb_5V$–Al catalyst shows Raman bands at 448, 384, 255, and 187 cm^{-1}, characteristic of α-Sb_2O_4, and a weak Raman band near 1024 cm^{-1}, characteristic of V=O bonds of dispersed tetrahedral VOx species. $0.50Sb_5V$–Al catalyst shows Raman bands at 188, 249, and 448 cm^{-1}, characteristic of Sb_2O_3, a weak Raman band at 1024 cm^{-1}, characteristic of V=O mode of dispersed tetrahedral VOx species. The used Sb–V–Al catalysts presented in Fig. 6, do not show the presence of Sb_2O_3 phase, in line with the trends underlined by XRD. Noticeably, $0.50Sb_5$ V–Al shows a significant increase of α–Sb_2O_4 and surface polymeric VOx species. $0.25V_5Sb$–Al shows no appreciable Raman bands.

Figure 7 shows the Raman spectra of fresh and used dehydrated alumina-supported Sb–V–O catalysts with loadings at the dispersion limit Sb/V atomic ratio. The catalysts with Sb/V molar ratio between 2 and 4 present very similar

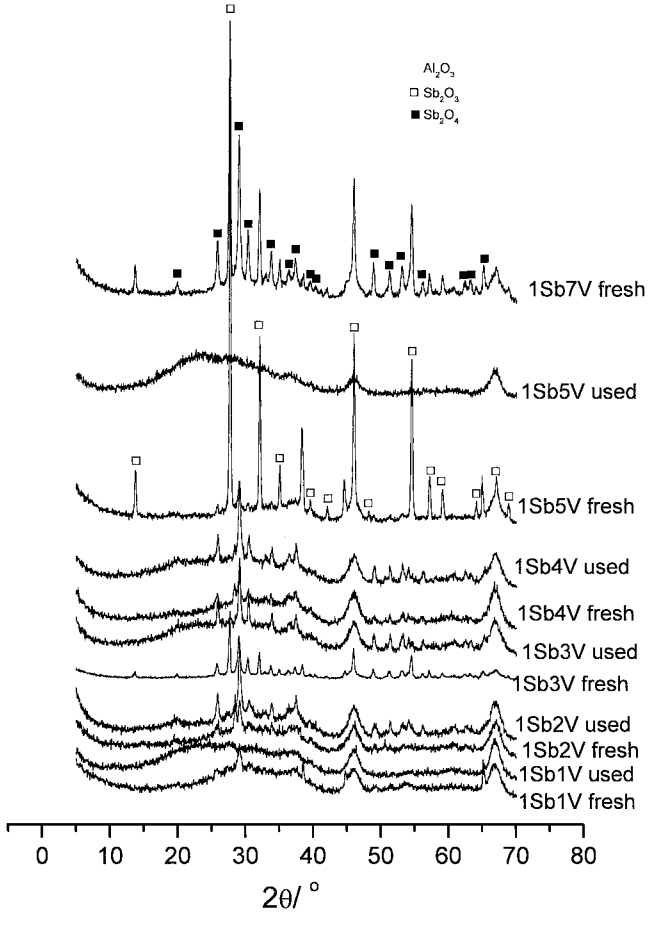

FIG. 3. XRD patterns of fresh and used catalysts at dispersion limit loading on alumina vs the atomic Sb/V ratio.

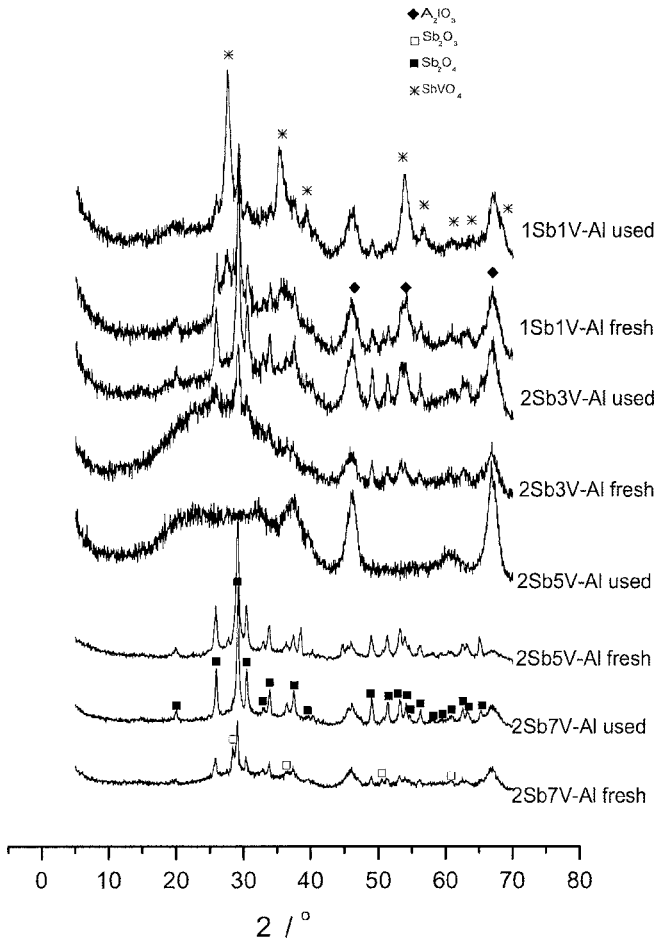

FIG. 4. XRD patterns of fresh and used catalysts at twice the dispersion limit loading on alumina vs the atomic Sb/V ratio.

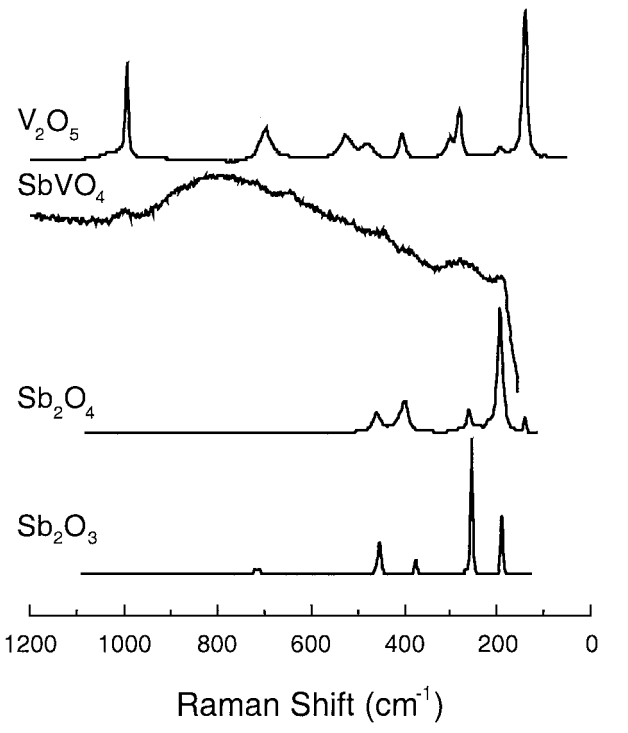

FIG. 5. Raman spectra of reference samples: Sb_2O_3, α-Sb_2O_4, $SbVO_4$, V_2O_5.

spectra: α-Sb_2O_4 dominates (because they have excess of antimony) and present a broad band near 800 cm^{-1}. But the catalyst with 1/1 Sb/V atomic ratio exhibits a broad band near 880 cm^{-1} and a weak band near 1024 cm^{-1}, typical of the V=O mode of tetrahedral surface VOx species. The band near 1024 cm^{-1} appears in the catalysts with 1/1, 2/1, and 3/1 Sb/V atomic ratio. This band is affected by hydration, which confirms that it belongs to surface dispersed VOx species. As Sb/V atomic ratio increases, the broad Raman band near 860 cm^{-1} shifts to ca. 796 cm^{-1}.

Figure 8 shows the Raman spectra of dehydrated fresh and used alumina-supported Sb–V–O catalysts at twice the dispersion limit loading for variable Sb/V atomic ratio. In some of the used catalyst the intensity of the bands from antimony oxides is smaller than that for the freshly prepared samples. The changes on Sb oxide species are less evident for $2Sb_1V$–Al due to the lower amount of Sb. However, the changes of the Raman bands of surface VOx species are very informative. The Raman band at 1024 cm^{-1} is almost absent after catalyst operation and the broad band of V–O–V vibration of surface polymeric VOx species shifts

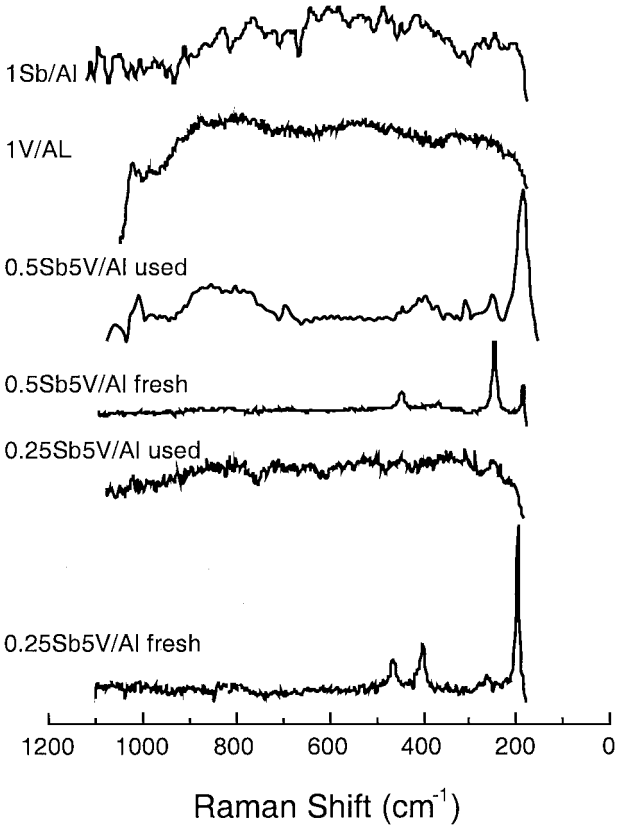

FIG. 6. Raman spectra of dehydrated fresh and used 1V–Al, 1Sb–Al, $0.25Sb_5V$–Al, and 0.50Sb5V–Al catalysts.

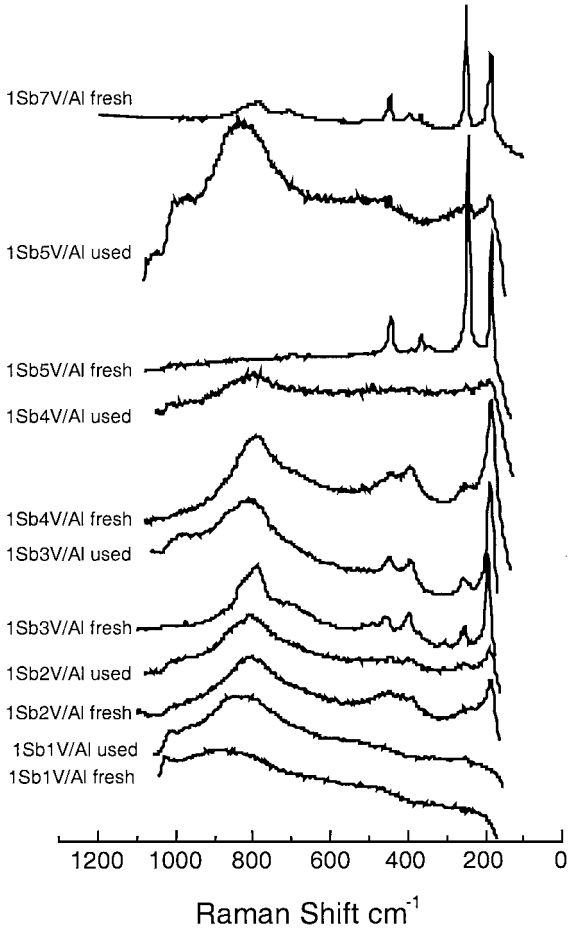

FIG. 7. Raman spectra of dehydrated fresh and used catalysts at dispersion limit loading on alumina vs the atomic Sb/V ratio.

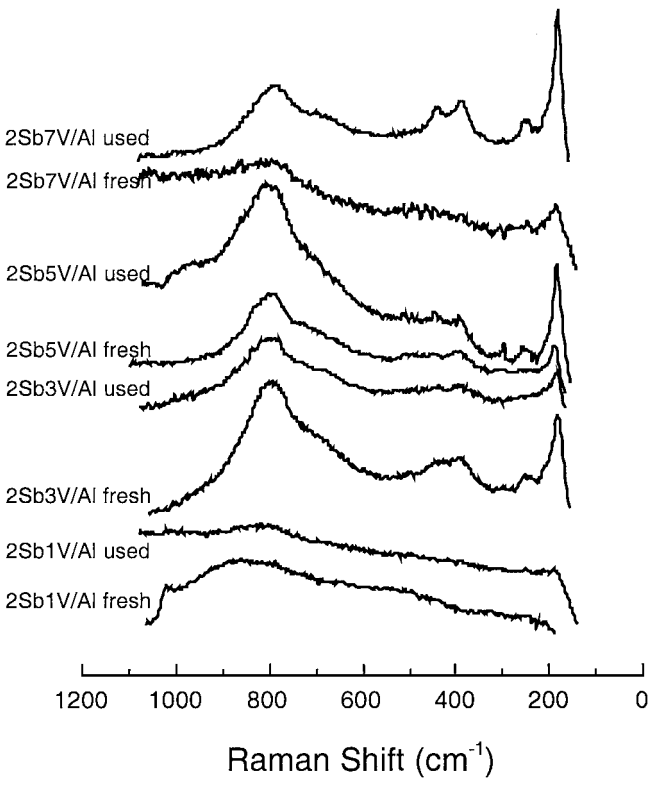

FIG. 8. Raman spectra of dehydrated fresh and used catalysts at twice dispersion limit loading on alumina vs the atomic Sb/V ratio.

to ca. 865 cm^{-1}. This broad Raman band further shift to ca. 798 cm^{-1}, as the Sb/V atomic ratio increases. The Raman spectra show a broad Raman band near 850 cm^{-1} and at 1024 cm^{-1} for fresh $2Sb_1V$–Al catalyst. After reaction, surface VOx species (1024 cm^{-1}) are no longer present and the broad Raman band at 850 cm^{-1} shifts to 865 cm^{-1}. This band is not sensitive to hydration. As Sb/V atomic ratio increases, the Raman band of α-Sb_2O_4 become more evident and the broad Raman band shifts closer to 798 cm^{-1}.

Effect of the Catalyst Composition

Table 2 shows the yield to the different products at 480°C for alumina, 1V–Al, 1Sb–Al, and $1Sb_1V$–Al. Alumina support has very low activity with poor selectivity, CO and CO_2 are the most important products, with acetonitrile as the only product of selective oxidation. The addition of Sb oxide to alumina (1Sb) minimizes the production of COx and yields tiny amount of acrylonitrile. The production of acetonitrile is not affected. When vanadium oxide is added to alumina (1V), the total activity of the system increases remarkably. Main products: $CO_2 > CO >$ acetonitrile $\gg$ propylene $\sim$ acrylonitrile $\gg$ acrolein $>$ ethylene. The presence of both Sb and V ($1Sb_1V$) on alumina affords very different catalytic profile. Main oxidation product is acrylonitrile (28% yield) $>$ propylene $\sim CO_2 \gg CO \gg$ acetonitrile. The product distribution is significantly different from that of 1V–Al or 1Sb–Al catalysts. Therefore, it does appear that V and Sb oxides combine to form a new catalytic phase, efficient for propane ammoxidation to acrylonitrile.

Behavior of the Catalysts vs Time-on-Stream (TOS)

The catalysts were tested against time on stream during at least 20 h at 480°C. Figure 9 presents the results for the

TABLE 2

Yield to Different Products on Alumina-Supported Catalysts

Product yield, %	Al_2O_3	1V–Al	1Sb–Al	$1Sb_1V$–Al
CO	5.13	22.78	0.00	11.28
CO_2	3.48	25.85	0.51	19.60
Propylene	0.57	2.72	0.00	20.51
Acetonitrile	1.54	19.93	1.33	4.97
Acrylonitrile	0.05	2.49	0.40	28.25
Acrolein	0.09	0.28	0.02	0.12

Note. Reaction conditions: 480°C, W = 200 mg, F = 20 ml/min (C_3H_8/O_2/NH_3/H_2O/He = 9.8/25/8.6/0/56.6 vol%).

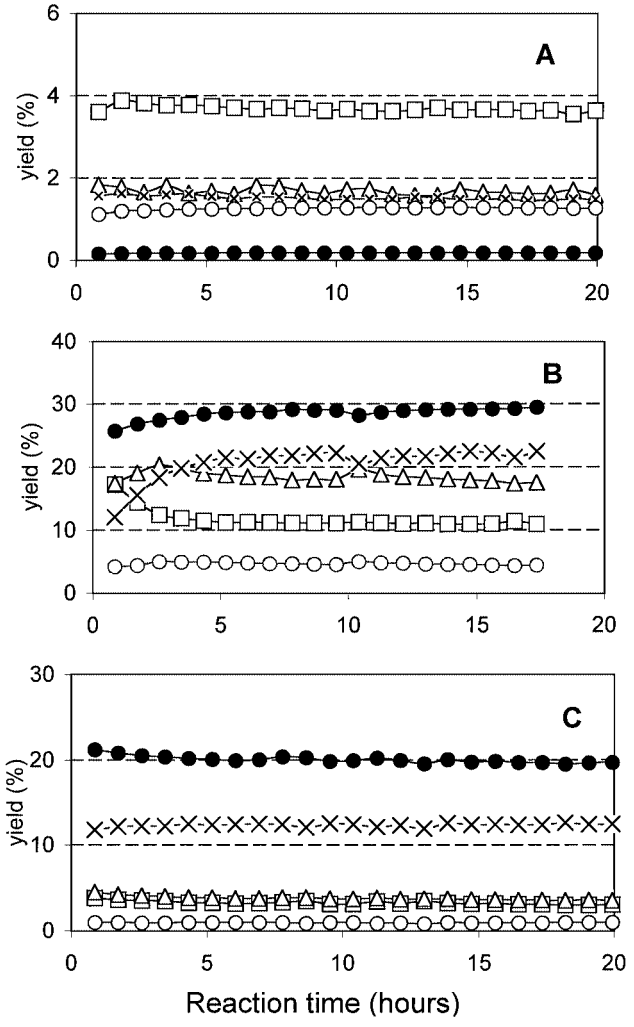

FIG. 9. Yield at 480°C vs time-on-stream for (A) 0.25Sb_5V–Al, (B) 1Sb_1V–Al, and (C) 2Sb5V–Al. Reaction conditions: total flow 20 ml/min; feed composition (% volume): $C_3H_8/O_2/NH_3/H_2O$/He (9.8/25/8.6/0/xx), 200 mg of catalyst. CO (square), CO_2 (triangle), propylene (x), acetonitrile (white circle), and acrylonitrile (solid circle).

representative 0.25Sb_5V–Al (Fig. 9A), 1Sb_1V–Al (Fig. 9B), and 2Sb_5V–Al (Fig. 9C) catalysts. At Sb + V loading below the dispersion limit on alumina, the activity and product distribution vs TOS remain constant (Fig. 9A). At dispersion limit loading of Sb + V on alumina, the catalysts show an increase in conversion values during the first 5 h, mainly due to a decrease in the yield to CO and a concomitant increase in the yields of propylene and of acrylonitrile mainly. The yield values to CO_2 and to acetonitrile do not appear to be affected (Fig. 9B). At twice the dispersion limit loading of Sb + V on alumina the catalyst shows steady state activity since the first hours of operation (Fig. 9C), and acrylonitrile is the main reaction product.

Total coverage of Sb + V on alumina results in different performance and trends during TOS operation. Figure 10 shows the effect of total Sb + V surface coverage on alumina on the yields to the different products at 480°C and on the specific rate of formation of acrylonitrile per vanadium site at 480°C. The main products for the catalysts at 25, 50, and at 100% dispersion limit loading and Sb/V = 5 atomic ratio are COx and propylene, but, with the same Sb/V molar ratio and with a coverage twice the dispersion limit loading, the main product is acrylonitrile. The number of mmol of acrylonitrile produced per mmol of vanadium in the bulk, i.e., the rate of the reaction per vanadium site is best for the catalyst with twice the dispersion limit loading on alumina at 5 Sb/V atomic ratio, which produces 10 mmol of acrylonitrile per mmol of vanadium and second.

Effect of Sb/V

Figure 11 shows the effect of Sb/V ratio on the yields to the different products and on the specific rate of formation of acrylonitrile per vanadium site at 480°C for catalysts at the dispersion limit loading of Sb + V on alumina. The catalysts with a large excess of antimony (Sb/V molar ratios of 5 and 7) present propylene as the main product and show a moderate deactivation during TOS. The catalysts with a moderate excess of Sb (Sb/V molar ratios of 3 and 5) present acrylonitrile like the main product and show a rather constant catalytic performance during TOS. The higher rates of reaction per vanadium site correspond to molar ratios of Sb/V = 3. It is interesting to note that fresh catalysts with a moderate excess of Sb show surface VOx species that would enable surface restructuring during on-stream operation affording better catalysts.

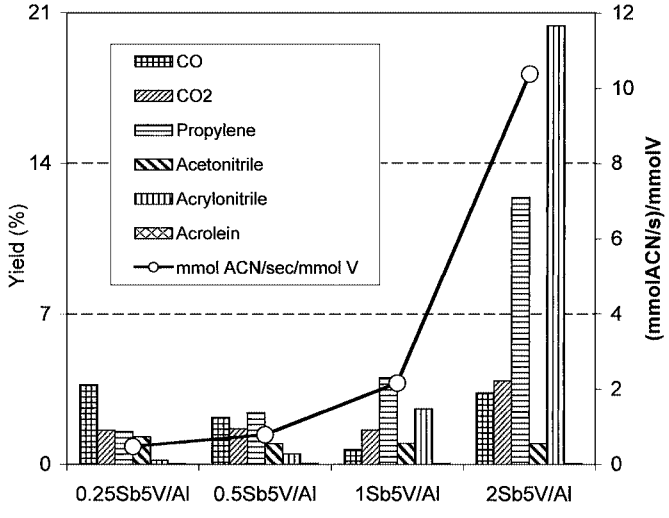

FIG. 10. Effect of total Sb + V coverage on alumina on the yields to different products and on the specific rate of formation of acrylonitrile per V site at 480°C. Reaction conditions: total flow 20 ml/min; feed composition (% volume): $C_3H_8/O_2/NH_3/H_2O$/He (9.8/25/8.6/0/56.6), 200 mg of catalysts.

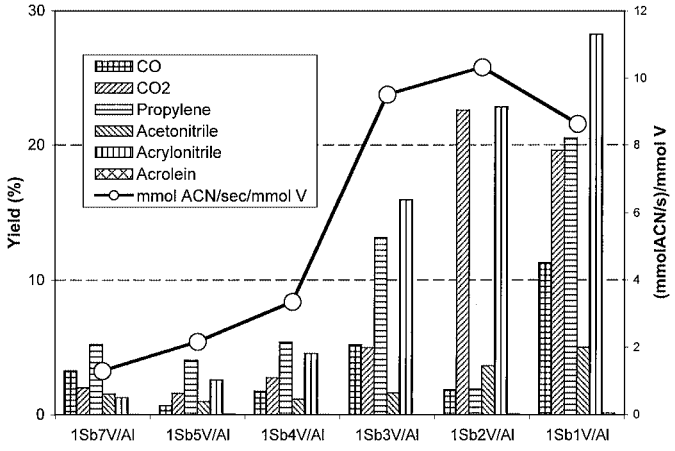

FIG. 11. Effect of total Sb/V atomic ratio on the yields to different products (left axis) and on the specific rate of formation of acrylonitrile per V site (right axis). Reaction conditions: total flow 20 ml/min; feed composition (% volume): $C_3H_8/O_2/NH_3/H_2O/He$ (9.8/25/8.6/0/56.6), 200 mg of catalyst.

However, at a large excess of Sb, no surface VOx species are present.

DISCUSSION

The *combination of Sb and V* appears critical to afford efficient catalysts. The performance of alumina support is highly inefficient for it produces mainly CO and CO_2. The incorporation of vanadium oxide species to alumina affords very active catalyst, but it mainly produces COx and cracking products in the form of acetonitrile. The incorporation of antimony oxide species to alumina depletes most of the nonselective activity, COx species are minimized and acetonitrile is the main product, the activity is very low. The same trend for $SbOx/Al_2O_3$ was reported by Andersson *et al.* (26, 27) who observed that propane transformation must occur through a different mechanism than the redox of Sb–V–O catalysts. Sb–V–based catalysts show an activation period with time-on-stream under reaction conditions (28). It is shown that used catalysts show an enrichment of their external surface with antimony (28). The antimony-enriched $SbVO_4$ is considerably more selective than the pure phase to acrylonitrile (16, 29). It has also been proposed that Sb–V–O mixed oxide catalysts possess surface VOx species (30). Surface enrichment of Sb also has a promoting effect on other catalyst formulations, e.g., Sn–Sb–V–O system (31). The promotional effect of α-Sb_2O_4 on Sb–V–O catalysts appears to be due to the surface enrichment with antimony at the surface creating isolation to a suitable level of the V centers (29).

Some catalysts show an *activation period* during the first few hours of operation, and no additional activation is observed in successive runs. The activation period does not appear to be associated with surface adsorption of reaction intermediates (37). The activation period appears to correspond to a change in the structure of the catalyst. The transient activation of Sb–V-based catalysts is a common feature in literature (32). It has been associated with a partial reduction of V sites during on-stream operation. *In situ* Raman and *in situ* UV–Vis–DRS spectroscopic techniques during propane oxidation on supported vanadia catalysts show reduction of V sites (33). The activation period does not appear to be associated to surface adsorption or reaction intermediates. The structure of the *catalysts changes* as the characterization of used catalysts shows. In particular, Sb_2O_3 phase tends to react into more oxidized phases. Raman spectra and XRD show that the removal of Sb_2O_3 phase leads to the formation of the α-Sb_2O_4 phase and, in some cases, Sb–V–O phases Sb(V) and V(III) (25). Thus, it appears that there is an oxidation of Sb sites and a reduction of V sites, in line with additional formation of Sb–V–O phases. XRD studies of bulk Sb–V–O catalysts underline the additional formation of Sb–V–O phases from V and Sb oxides, which did not combine during calcination (34). Transmission electron microscopy shows that used bulk Sb–V–Al-based catalysts present aggregates of rutile-type phase crystal more frequently in the used samples, and they were rather difficult to observe in the fresh samples (28). This rutile phase does not include Al (28). The structural change of Sb–V–O catalysts may be induced by the interaction with reaction media (35). However, Knözinger and coworkers have very recently shown that the interaction between Sb and V can be induced by moisture on titania-supported Sb–V–O systems, affording the formation of Sb–V–O phases (36).

At low surface coverage (25% of dispersion limit loading), catalyst $0.25Sb_5V$–Al has α-Sb_2O_4 phase and dispersed surface vanadium oxide species (Fig. 6), but no significant Raman bands are observed in the used catalyst. At medium surface coverage (50% of dispersion limit on alumina), catalyst $0.5Sb_5V$–Al shows the Raman bands of Sb_2O_3, no appreciable bands of vanadium oxide species are recorded. Intuitively, it could be assumed that some coordination between Sb and V may prevent the existence of surface vanadium oxide species. The Raman bands of $VSbO_4$ phases are weak, and it is likely that its presence cannot be detected on these samples. However, the structural rearrangement during the catalytic run results in new Raman bands for the used catalysts at 180 and 250 cm^{-1}, characteristic of α-Sb_2O_4, and also those of surface polymeric vanadium oxide species at 1024 cm^{-1} (V=O mode) and near 890 cm^{-1} (V–O–V mode). It is possible that below the dispersion limit coverage, any Sb–V–O phase that may be present on the fresh catalyst would break and disperse on the support. The Raman spectra of used $0.50Sb_5V$–Al shows Raman bands of α-Sb_2O_4 and of surface polymeric VOx species. Since the fresh catalyst did not show Raman bands of surface VOx species, it must be due to coordination between Sb and V as

$SbVO_4$ phases (weak Raman signal). Therefore, it appears that below the dispersion limit loading on alumina, $SbVO_4$ phases are not stable and break into its constituting oxides during on-stream operation.

The Raman spectra of Sb–V–Al–O catalysts at dispersion limit loading shows the bands of surface polymeric and isolated vanadium oxide species; however, no bands can be assigned to antimony oxide phase. The XRD patterns show that this catalyst possesses α-Sb_2O_4. The used catalysts present a very broad pattern near 25°. The most intense diffraction peak of $Sb_xV_{1-x}O_{4-1.5x}$ phase lies near 28°. Thus, this broad feature could be indicative on an incipient Sb–V–O phase. The Raman spectra of this catalyst show an important decrease of V=O groups of dispersed vanadium oxide species and a shift of the broad band near 890 to 850 cm^{-1}. As the Sb/V atomic ratio increases for the alumina-supported Sb–V catalysts at dispersion limit coverage, the Raman bands of α-Sb_2O_4 become more evident. Interestingly, the presence of surface vanadium oxide species decreases after catalytic runs and the broad Raman band at 890 cm^{-1} shifts concomitantly to lower values. In particular, the new Raman band is sensitive to the Sb/V atomic ratio for it shifts from ca. 850 cm^{-1} (used $1Sb_1V$–Al) to ca. 810 cm^{-1} (used $1Sb_2V$–Al and $1Sb_3V$–Al); and further shifts to ca. 800 cm^{-1} ($1Sb_4V$–Al and $1Sb_7V$–Al). The used catalysts show little or no surface vanadium oxide species left. The Raman band near 798 cm^{-1} cannot correspond to surface vanadium oxide species, since no Raman band is present at 1024 cm^{-1}. The reference $SbVO_4$ sample shows a broad Raman band at 800 cm^{-1}. Thus, the band at 800 cm^{-1} underlines the formation of $SbVO_4$ phases. At lower Sb/V atomic ratio values, the presence of $SbVO_4$ must account for the shift to lower Raman shift of the broad Raman band near 890 cm^{-1}. Thus, the broad Raman band shifting from 890 to 800 cm^{-1} with Sb/V atomic ratio on used catalysts must be a linear combination of the Raman bands of surface polymeric vanadium oxide species near 890 cm^{-1} and that of the $SbVO_4$ phase at 800 cm^{-1}. However, the presence of $SbVO_4$ phases is not affording higher yield values to acrylonitrile at high Sb/V atomic ratio values. This is probably due to a coverage of $SbVO_4$ phases by surface Sb species. Thus, a moderate excess of Sb (near Sb/V = 3) would be beneficial for propane ammoxidation to acrylonitrile, while a large excess of Sb may lead to a blockage of $SbVO_4$ sites.

At a Sb + V surface coverage twice the dispersion limit on alumina, the interaction between surface antimony oxide and vanadium oxide phases after the catalytic run becomes most evident. Actually, Sb–V–O phase in catalyst $2Sb_1$ V–Al is large enough to produce a diffraction pattern (Fig. 4). The Raman spectra of fresh and used catalysts with Sb + V coverage of twice the dispersion limit value show the formation of Sb–V–O phase by a Raman band near 800 cm^{-1}, which is sharper than for the series at dispersion limit coverage. Comparison of the Raman spectra of fresh and used catalyst shows the loss of surface vanadium oxide species during the catalytic runs.

The reaction performance mirrors the structural transformations during on-stream operation. Thus, representative catalyst $1Sb_1V$–Al (Fig. 9B) shows a continuous decrease in the formation of CO (from ca. 17 to 10% yield) and a complementary increase in the yield values to propylene (from 12 to 22% yield) and to acrylonitrile (from 26 to 29% yield). Then, the catalyst appears to reach a steady-state operation. Below the dispersion limit coverage, no Sb–V–O phase appears to form. Some fresh catalysts appear to have some Sb–V–O phase, but it breaks and disperses into surface vanadium oxide and antimony oxide. Thus, these systems afford very poor performance for propane ammoxidation and their activity during TOS appears to remain constant at a low performance level. This is illustrated in Fig. 9A for representative catalyst $0.25Sb_5V$–Al. No transient deactivation is recorded for this catalyst, the destruction of the Sb–V–O phase for catalysts below the dispersion limit must be very fast.

From the structural information on the relevance of Sb + V coverage on alumina, it is easy to understand how catalysts with surface coverage below the dispersion limit on alumina show modest performance toward propane ammoxidation (Fig. 10). Below the dispersion limit, acrylonitrile is a minor product. However at the dispersion limit on alumina, acrylonitrile becomes the main product. At twice the dispersion limit coverage, the total activity and selectivity is significantly higher. Most important, the specific activity per vanadium site is maximum (increases by a factor of 20 in the series). The improvement of performance toward acrylonitrile runs parallel to the presence of the Sb–V–O phases. Thus, it is clear that the presence of Sb–V–O phases is essential for propane ammoxidation to acrylonitrile.

CONCLUSIONS

The presence of Sb–V–O phase is essential for the ammoxidation of propane to acrylonitrile on alumina-supported Sb–V oxide catalysts. The structure and performance of alumina-supported V + Sb catalysts is determined by both Sb + V surface coverage and Sb/V atomic ratio. The final structure of the catalyst is attained during the catalytic process. At low surface coverage, supported Sb–V–O phase is not stable during reaction and tends to break into the individual oxides that disperse as surface oxide species. These catalysts show very little activity. Their structural breakdown must be very fast since no deactivation is recorded during the initial hours of operation. When surface Sb + V coverage reaches dispersion limit, surface vanadium oxide species and antimony oxide species tend to combine into Sb–V–O phase during catalytic operation, as reflected by the used catalysts. This interaction must take

place during the first few hours of catalytic operation, while both propane conversion and acrylonitrile selectivity increase. The extent of Sb–V–O phase formation increases with Sb + V loading if it is beyond the dispersion limit value. The more extended the formation of Sb–V–O phase is, the higher the yield to acrylonitrile and the specific rate of acrylonitrile formation per V site are. The Sb/V atomic ratio also determines the performance of alumina-supported Sb–V–O catalysts above the dispersion limit on alumina. At very high Sb/V atomic ratio, total acrylonitrile and specific activity per vanadium site remain very low, probably due to coverage of active sites by excess Sb. Both acrylonitrile yield and specific rate per vanadium site increase as Sb/V atomic ratio decreases. The specific formation of acrylonitrile per vanadium site reaches a maximum at an Sb/V atomic ratio of 2. It is likely that a moderate excess of antimony may be necessary for an efficient ammoxidation of propane to acrylonitrile.

ACKNOWLEDGMENTS

This research was funded by CICYT, Spain, under PROJECT QUI98-0784, and Repsol-YPF, Spain. Spanish CICYT Grant IN96-0053 funded, in part, the acquisition of the Raman spectroscopic system. M.O.G.-P. thanks the Ministry of Science and Technology of Spain for a doctorate studies fellowship.

REFERENCES

1. *Chemical Week*, p. 5 (June 4, 1997).
2. Bowker, M., Bicknell, C. R., and Kerwin, P., *Appl. Catal. A* **136**, 205 (1996).
3. Sokolovskii, V. D., Davydov, A. A., and Ovsitser, O. Yu., *Catal. Rev.* **37**, 425 (1995).
4. Kim, Y.-C., Ueda, W., and Moro-oka, Y., *Appl. Catal.* **70**, 189 (1991).
5. Centi, G., Grasselli, R. K., and Trifirò, F., *Catal. Today* **13**, 661 (1992).
6. Grasselli, R. K., *Catal. Today* **49**, 141 (1999).
7. Centi, G., Perathoner, S., and Trifirò, F., *Appl. Catal. A* **157**, 143 (1997).
8. Centi, G., Marchi, F., and Perathoner, S., *Appl. Catal. A* **149**, 225 (1997).
9. Brazdil, J. F., Bartek, J. P., U.S. Patent 5,854,172 (1998); Brazdil, J. F., Kobarvkantei, F. A. P., Padolwski, J. P., JP Patent 11033399 (1999); Guttmann, A. T., Grasselli, R. K., and Brazdil, F. J., U.S. Patents 4,746,641; 4,788,173; 4,837,233 (1988).
10. Brazdil, J. F., Calvalcanti, F. A. P., EP Patent 0765684 (1997); Cavalcanti, F. A. P., Bremer, N. L., Brazdil, J. F., Brazdil, L. C., WO Patent 9505895 (1995).
11. Kim, Y.-C., Ueda, W., and Moro-oka, Y., *Catal. Today* **13**, 673 (1992).
12. Sureh, D. D., Ornoff, D. A., Brazdil, J. F., Glaeser, L. C., and Friendich, M. S., U.S. Patent 4,7060,159 (1988).
13. Glaeser, L. C., Brazdil, J. F., Toft, M. A., U.S. Patents 4,843,655; 4,835,125 y 4,837,192 (1988).
14. Kim, J. S., and Woo, S. I., *Appl. Catal. A* **110**, 207 (1994).
15. Ushikubo, T., Oshima, K., Kayou, A., Vaarkamp, M., and Hatano, M., *J. Catal.* **169**, 394 (1997).
16. Nilsson, R., Lindblad, T., and Andersson, A., *J. Catal.* **148**, 501 (1994); Nilsson, R., Lindblad, T., Andersson, A., Song, C., and Hansen, S., *Stud. Surf. Sci. Catal.* **82**, 293 (1994).
17. Centi, G., and Perathoner, S., *Catal. Rev.* **40**, 175 (1998).
18. Centi, G., Perathoner, S., *Chemtech*, Feb. 13, 1998.
19. Zanthoff, H. W., Buchholz, S. A., and Ovsitser, O. Y., *Catal. Today* **32**, 291 (1996).
20. Vaarkamp, M., and Ushikubo, T., *Appl. Catal. A* **174**, 99 (1998).
21. Brazdil, L. C., Ebner, A. M., and Brazdil, J. F., *J. Catal.* **163**, 117 (1996).
22. Albonetti, S., Blanchard, G., Burattin, P., Cassidy, T. J., Masetti, S., and Trifirò, F., *Catal. Lett.* **45**, 119 (1997).
23. Zanthoff, H. W., and Buchhoz, S. A., *Catal. Lett.* **49**, 213 (1997).
24. Wachs, I. E., Briand, L. E., Jehng, J.-M., Burcham, L., and Gao, X., *Catal. Today* **57**, 323 (2000).
25. Birchall, T., and Sleight, A. W., *Inorg. Chem.* **15**(4), 868 (1976).
26. Andersson, A., Andersson, S. L. T., Centi, G., Grasselli, R. K., Sanati, M., and Trifirò, F., *Stud. Surf. Sci. Catal.* 691 (1993).
27. Andersson, A., Andersson, S. L. T., Centi, G., Grasselli, R. K., Sanati, M., and Trifirò, F., *Appl. Catal. A* **113**, 43 (1994).
28. Nilsson, J., Landa-Cánovas, A. R., Hansen, S., and Andersson, A., *J. Catal.* **186**, 442 (1999).
29. Nilsson, J., Landa-Cánovas, A. R., Hansen, S., and Andersson, A., *Catal. Today* **33**, 97 (1997).
30. Zanthoff, H. W., Grünert, W., Buchholz, S., Heber, M., Stievano, L., Wagner, F. E., and Wolf, G. U., *J. Mol. Catal. A* **162**, 443 (2000).
31. Albonetti, S., Blanchard, G., Burattin, P., Cavani, F., Masetti, S., and Trifirò, F., *Catal. Today* **42**, 283 (1998).
32. Centi, G., and Perathoner, S., *Appl. Catal. A* **124**, 317 (1995).
33. Gao, X., Jehng, J.-M., and Wachs, I. E., submitted for publication.
34. Centi, G., Foresti, E., and Guarnieri, F., *Stud. Surf. Sci. Catal.* **82**, 281 (1994).
35. Nilsson, R., Landa-Cánovas, A. R., Hansen, S., and Andersson, A., *J. Catal.* **160**, 244 (1996).
36. Schubert, U.-A., Anderle, F., Spengler, J., Zühlke, Eberle, H.-J., Grasselli, R. K., and Knözinger, H., *Topics Catal.* **15**, 195 (2001).
37. Guerrero-Pérez, M. O., Fierro, J. L. G., Peña, and Bañares, M. A., in preparation.